Fracture toughness and crack-growth measurements in GRP

M. J. OWEN, R. J. CANN*
Department of Mechanical Engineering, University of Nottingham, Nottingham, UK

Critical crack tip stress intensity factor (K_c) measurements were made for polyester resin reinforced with glass chopped strand mat (CSM) and woven roving fabric (WRF). Specimen thickness and initial crack length were varied for centre notched (CN) 100 mm wide specimens. Some specimens were saturated by immersion in water under pressure. K_c was negligibly affected by specimen thickness and it was concluded that plane strain conditions are not achieved in laminates of normal thickness. Scatter can be reduced by adjusting results to a standard glass content and K_c varies continuously with crack length. The CSM experiments were extended to 915 mm wide specimens which failed at very low nett section stresses but there may be a region in which K_c is roughly constant relative to crack length. In WRF specimens, however, it is the nett section stress which is constant at a value substantially below the UTS. Fatigue crack-growth studies were carried out on CN specimens. The Paris law adequately describes crack growth in CSM specimens at low rates of growth but Forman's law is better at high rates of growth. Neither law is valid for WRF material when dry but the behaviour changes after saturation with water. The crack-growth resistance of both materials is severely reduced by saturation with water.

1. Introduction

For both brittle and ductile materials, it is often possible to predict the failure of cracked components subjected to static or cyclic loads using the principles of fracture mechanics [1, 2]. In recent years there have been attempts to apply this growing body of work to glass-reinforced plastics (GRP). The aims of the work described here were to examine the problems associated with the application of linear elastic fracture mechanics to static and fatigue failure in GRP, both dry and after a period of immersion in water.

Table I summarizes the GRP fracture toughness results obtained by a number of investigators [3–15]. The parameters commonly measured are critical stress intensity factor, K_c, and critical strain energy release rate G_c. It can be seen from Table I that these quantities are dependent on:

(1) glass content (glass content variation is indicated by different ultimate tensile strengths for similar materials);
(2) specimen type;
(3) specimen size;
(4) crack length;
(5) reinforcement type.

G_c values determined by compliance methods differed from those calculated from K_c values unless they had been corrected to allow for crack tip damage [13] by adding a small amount to the crack length used to calculate K_c. This incremental crack length was either measured [3, 7], or Irwin's correction was applied [7, 9], i.e. by adding r_y to the initial crack length, where

$$r_y = \frac{1}{c}\left(\frac{K}{\sigma_y}\right)^2 \quad (1)$$

where $c = \frac{1}{2}\pi$ for plane stress or $\frac{1}{6}\pi$ for plane strain, and σ_y is the yield stress. Since GRP do not yield, various stresses have been used for σ_y, and attempts have been made to relate them to observed values, [9, 10, 13, 14]. Because corrections increased K_c values between 10 and 70%, for comparison purposes uncorrected values appear in Table I. Results taken from various sources [3, 5, 7, 9, 13] are plotted in Fig. 1.

Reductions in strength and stiffness of about

* Present address: National Coal Board, Mining Research and Development Establishment.

0022–2461/79/081982–15 $03.50/0

TABLE I Survey of GRP fracture toughness results

	Reinforcement	Matrix	UTS (MPa)	S_{11} (GPa^{-1})	CN t (mm)	CN a (mm)	CN W (mm)	CN K_c (MPa m$^{1/2}$)	CN G_c (kJ m^{-2})	DEN t (mm)	DEN a (mm)	DEN W (mm)	DEN K_c (MPa m$^{1/2}$)	DEN G_c (kJ m^{-2})	SEN t (mm)	SEN a (mm)	SEN W (mm)	SEN K_c (MPa m$^{1/2}$)	SEN G_c (kJ m^{-2})	BEND t (mm)	BEND a (mm)	BEND W (mm)	BEND K_c (MPa m$^{1/2}$)	BEND G_c (kJ m^{-2})
[3]	Unidirectional	Epoxy			1.27	6.73	152	1.84																
					1.27	19.30	152	1.69																
					1.27	3.05	152	1.42																
					1.27	19.43	152	1.73																
					1.27	18.80	152	1.84																
					1.27	18.92	152	1.67																
					1.27	6.86	152	1.55																
					1.27	6.86	152	1.63																
					1.27	14.61	152	1.84																
					1.27	12.95	152	1.80																
					1.27	12.70	152	1.71																
					1.27	12.70	152	1.81																
					1.27	2.92	152	1.56																
					1.27	2.92	152	1.30																
					1.27	4.19	152	1.51																
					1.27	3.18	152	1.50																
					1.27	6.35	152	1.61																
					1.27	6.73	152	1.65																
					1.27	6.86	152	1.53																
					1.27	12.70	152	1.76																
					1.27	12.75	152	1.63																
					1.27	12.45	152	1.83																
[4]	Unidirectional																							
	S-HTS	EPON 826/CL								2.54		76.2	1.187	0.1751	2.54		38.1	1.396	0.1576					
	E-HTS	ERL 2256/0820								2.54		76.2	1.439	0.2277	2.54		38.1	1.670	0.2102					
	E-HTS	EPON 826/CL								2.54		76.2	1.209	0.1926	2.54		38.1	1.472	0.2802					
	E-HTS	ERL 2256/0820								2.54		76.2	0.9340	0.0525	2.54		38.1	1.132	0.0525					
	S-HTS	EPON 826/CL (B-staged)								2.54		76.2	0.2967	0.0525	2.54		38.1	0.3516	0.0876					
	S-HTS	EPON 826/MABA								2.54		76.2	1.374	0.5249	2.54		38.1	1.626	0.4904					
[5]	Random	Polyester		0.1587						G 1.5	1.25	25.0	6.93	7.62						1.5	1.05	10.00	10.1	16.2
	chopped									G 1.5	2.50	25.0	9.68	14.86						1.5	3.05	10.00	9.4	14.0
	E-glass									G 1.5	3.75	25.0	10.27	16.74						1.5	4.80	10.00	10.0	16.0
	fibres									G 1.5	5.00	25.0	9.35	13.86						3.5	1.30	10.00	9.9	15.4
	G refers									3.5	1.25	25.0	4.39	3.06						3.5	2.90	10.00	9.9	15.6
	to grooved									3.5	2.50	25.0	6.04	5.80						3.5	4.85	10.00	9.4	14.0
	specimens									3.5	3.75	25.0	6.58	6.88						1.5	1.00	10.00	8.1	10.4
										3.5	5.00	25.0	6.41	6.52						1.5	0.30	10.00	7.9	10.0
										3.5	6.25	25.0	5.59	4.96						1.5	4.80	10.00	9.1	14.0
										1.5	4.38	25.0	5.99	5.70						3.5	1.30	10.00	7.8	9.8
										1.5	3.95	25.0	8.15	10.55						3.5	0.29	10.00	7.9	10.0
																				3.5	4.80	10.00	7.1	8.0

TABLE I (Continued)

	Reinforcement	Matrix	UTS (MPa)	S_{11} (GPa^{-1})	CN t (mm)	CN a (mm)	CN W (mm)	CN K_c ($MPa\,m^{1/2}$)	CN G_c ($kJ\,m^{-2}$)	DEN t (mm)	DEN a (mm)	DEN W (mm)	DEN K_c ($MPa\,m^{1/2}$)	DEN G_c ($kJ\,m^{-2}$)	SEN t (mm)	SEN a (mm)	SEN W (mm)	SEN K_c ($MPa\,m^{1/2}$)	SEN G_c ($kJ\,m^{-2}$)	BEND t (mm)	BEND a (mm)	BEND W (mm)	BEND K_c ($MPa\,m^{1/2}$)	BEND G_c ($kJ\,m^{-2}$)
[6]	S-glass	Scotchply	145.0	0.0117	G 1.0	8.2	25.4	95.3															143.00	242.00
	unidirectional	Epoxy			G 1.0	9.0	25.4	96.0																
					G 1.0	9.9	25.4	76.5																
					G 1.0	10.5	25.4	51.0																
[7]	Scotchply	Epoxy		0.0433							2.4	25.4	25.10											
	1002										2.4	25.4	28.93											
	unidirectional										2.54	25.4	27.95											
											2.59	31.7	26.63											
											5.08	31.7	21.92											
	90°/0°/0°										5.08	31.7	27.40											
	90°										5.08	31.7	28.93											
											7.62	31.7	25.65											
											7.62	31.7	26.52											
											7.62	31.7	23.78											
											7.87	31.7	27.07											
	Scotchply	Epoxy		0.0363							6.35	38.1	50.20											
	1002										6.73	38.1	43.29											
	unidirectional										9.52	38.1	44.17											
											9.52	38.1	42.63											
	90°/0°/0°										9.93	38.1	43.29											
	0°/90°										10.67	38.1	49.89											
											5.08	50.8	41.32											
											6.35	50.8	39.68											
											9.14	50.8	46.80											
	1 ply	Epoxy			0.25	0.25	38.1	8.4		0.25	1.04	38.1	18.4											
	181-style	and			0.25	0.64	38.1	11.2		0.25	1.78	38.1	18.2											
	balanced	polyester			0.25	1.04	38.1	12.9		0.25	2.52	38.1	18.2											
	weave				0.25	1.02	38.1	14.0		0.25	2.54	38.1	19.8											
	fabric				0.25	1.27	38.1	14.8		0.25	2.54	38.1	17.3											
					0.25	1.70	38.1	16.4		0.25	3.56	38.1	16.0											
					0.25	2.29	38.1	15.8		0.25	5.72	38.1	18.4											
					0.25	3.30	38.1	17.8		0.25	6.35	38.1	19.3											
					0.25	4.98	38.1	18.2		0.25	6.35	38.1	20.6											
					0.25	6.20	38.1	17.8																
	Random	Polyester								1.78	2.29	25.4	6.96											
	chopped									1.78	2.79	25.4	8.06											
	fibres									1.78	3.56	25.4	8.42											
	6-plies									1.78	3.30	25.4	7.52											
										1.78	3.56	25.4	8.48											
										1.78	5.33	25.4	8.35											
										1.78	4.57	25.4	9.51											
										1.78	5.01	25.4	9.27											
[8]	Unidirectional	Epoxy			0.889	25.4	25.4	13.63		0.889	101.6	25.4	19.57											
	60°/60°/60°				1.651	25.4	25.4	15.72		1.651	121.6	25.4	16.48											

TABLE I (Continued)

	Reinforcement	Matrix	UTS	S_{11}	CN					DEN					SEN					BEND				
			(MPa)	(GPa^{-1})	t (mm)	a (mm)	W (mm)	K_c (MPa m$^{1/2}$)	G_c (kJ m^{-2})	t (mm)	a (mm)	W (mm)	K_c (MPa m$^{1/2}$)	G_c (kJ m^{-2})	t (mm)	a (mm)	W (mm)	K_c (MPa m$^{1/2}$)	G_c (kJ m^{-2})	t (mm)	a (mm)	W (mm)	K_c (MPa m$^{1/2}$)	G_c (kJ m^{-2})
[9]	A Supremat	Polyester	137.0	0.101						3.2	12.50	75.0	10.47											
	E-glass CSM									3.2	16.67	100.0	11.08											
	3-plies									3.2	25.00	150.0	11.80											
										4.54	100.00	600.00	15.65											
	Tyglass Y221 E-glass A1100 Silane finish 9-plies	Polyester																						
	B – 0°		402.0	0.0354						2.79	12.50	75.0	42.44											
										2.79	16.67	100.0	42.44											
										2.79	25.00	150.0	47.27											
	B – 0°		52.4	0.0894						2.79	12.50	75.0	4.73											
										2.79	16.67	100.0	4.73											
										2.79	25.00	150.0	4.73											
										3.09	100.00	600.0	6.31											
	C Tyglass	Polyester	229.0	0.0487						3.09	12.50	75.0	19.60											
	Y449									3.09	16.67	100.0	20.98											
	Silane finish									3.09	25.00	150.0	22.70											
	7-plies																							
[10]	None	Polyester	52.9	0.2597	1.25	12.7	76.2	0.825																
			52.9	0.2597	8.00	12.7	76.2	0.699																
	CSM FGE 200 E-glass 1 ply	Polyester	78.9		1.25	12.7	76.2	9.61																
	Tyglass Y227 E-glass 1 ply	Polyester	255.4		1.25	12.7	76.2	13.63																
[11]	CSM Supremat	Polyester	85.0	0.1205	5.8	10.0	100.0		20.65															
	6-plies				5.8	15.0	100.0		19.61															
					5.8	20.0	100.0		17.79															
					5.8	25.0	100.0		17.20															
[12]	M(CSM) + R(WRF 779-style) as M/R/M/R/M	Polyester		0.0545											5.49	Various	114.3	19.30						
[13]	CSM	Polyester	85.0	0.1205	5.8	10.0	100.0	8.81		5.8	10.0	100.0	8.39							6.0	30.0	150.0	5.64	
					5.8	15.0	100.0	9.43		5.8	15.0	100.0	8.12							6.0	40.0	200.0	6.63	
					5.8	20.0	100.0	9.78		5.8	20.0	100.0	8.86							6.0	50.0	250.0	6.64	
					5.8	25.0	100.0	8.91		5.8	25.0	100.0	9.98											
					5.8	15.0	100.0	9.43		5.8	15.0	100.0	8.12											
					5.8	22.5	150.0	8.98		5.8														
					5.8	30.0	200.0	8.60																
					5.8	37.5	250.0	9.16		5.8	37.5	250.0	10.04											
					5.8	90.0	600.0	10.66																
	CSM	Urethane	67.7	0.0599																6.0	30.0	150.0	5.63	
																				6.0	40.0	200.0	6.21	
																				6.0	50.0	250.0	6.24	

TABLE I (Continued)

Ref.	Reinforcement	Matrix	UTS (MPa)	S_{11} (GPa^{-1})	CN					DEN					SEN					BEND				
					t (mm)	a (mm)	W (mm)	K_c (MPa m$^{1/2}$)	G_c (kJ m^{-2})	t (mm)	a (mm)	W (mm)	K_c (MPa m$^{1/2}$)	G_c (kJ m^{-2})	t (mm)	a (mm)	W (mm)	K_c (MPa m$^{1/2}$)	G_c (kJ m^{-2})	t (mm)	a (mm)	W (mm)	K_c (MPa m$^{1/2}$)	G_c (kJ m^{-2})
	Tyglass	Polyester	202.3	0.1880	3.6	10.0	100.0	17.14		3.6	10.0	100.0	16.10											
	Y449				3.6	15.0	100.0	17.72		3.6	15.0	100.0	17.90											
					3.6	20.0	100.0	17.29		3.6	20.0	100.0	18.88											
					3.6	25.0	100.0	16.91		3.6	25.0	100.0	17.88											
					3.6	15.0	100.0	17.72		3.6	15.0	100.0	17.90											
					3.6	22.5	150.0	19.86		3.6										3.6	30.0	150.0	13.99	
					3.6	30.0	200.0	20.33		3.6										3.6	40.0	200.0	15.14	
					3.6	37.5	250.0	21.58		3.6	37.5	250.0	23.14							3.6	50.0	250.0	17.76	
[14]	CSM 3 plies	Epoxy	160												3.18	5.08	25.4	13.42						
[15]	Unidirectional	Epoxy	1295												3.10	12.7	25.4	14.4						

Nomenclature

CN	Centre notch specimens	S_{11}	Minimum normal material compliance
DEN	Double edge-notch specimens	t	Specimen thickness
SEN	Single edge-notch specimens	a	Crack length (half crack length in CN specimens)
Bend	3 or 4-point bend specimens	W	Specimen width
UTS	Ultimate tensile strength	K_c	Uncorrected critical stress intensity factor (Mode I)
CSM	Chopped strand mat	G_c	Critical strain energy release rate
		G	Suffix in thickness column indicates grooved specimens

K_c are uncorrected values, calculated by the author where not given in the reference. Corrected values are discussed in the text (Section 2.3).

10% have been recorded in GRP immersed for long periods in water at room temperature [16, 17]. The ability of filament-wound GRP to maintain its stiffness when subjected to cyclic loading under water has been shown to depend on the strength of the glass–resin bond [18].

The Paris crack-propagation law [19] has been applied to several types of composite materials [20–23]. Values of A and m in the equation

$$\frac{da}{dN} = A(\Delta K)^m \qquad (2)$$

have been determined for some GRP up to 20 000 cycles [23].

The main conclusions to be drawn from the survey are as follows:

(1) many of the published results have been derived from small specimens;

(2) the correlation between G_c and K_c results is poor;

(3) for some materials, e.g. chopped strand mat reinforced polyester resin, there seems to be a marked size effect which could suggest the relevance of fracture mechanics concepts;

(4) the conditions for valid fracture toughness testing of GRP have not yet been established.

2. Materials and test methods

The materials examined in the present work were (i) polyester resin reinforced with chopped strand mat (CSM/PR), and (ii) polyester resin reinforced with woven roving fabric (WRF/PR). The details are given in Table II. Laminates were laid up by hand, then left for 3 days at room temperature before post-curing for 3 days at 40° C, and then cut into specimens with a diamond-impregnated slitting wheel. The strength and stiffness properties of the materials were determined using the tensile and plate twist specimens shown in Fig. 2 and are summarised in Table III.

Glass content by weight was determined by burning the resin from weighed samples cut from test specimens in a muffle furnace, then weighing the remaining glass. Using the least squares method, straight lines were fitted to plots of strength, stiffness, and fracture toughness versus glass content. This adequately described the variation of these properties over the range of glass content encountered in the work.

To simulate the effect of several years immersion in water, specimens were conditioned in tap water at ambient temperature under a pressure of 6.9 MPa for 16 weeks. The water absorption was found to be independent of specimen type or size. For CSM/PR and WRF/PR the increase in weight due to water absorbed was 1.2 and 0.6%, respectively. Water damage took the form of patches of debonded fibres evenly distributed over the specimens. There were no resin cracks.

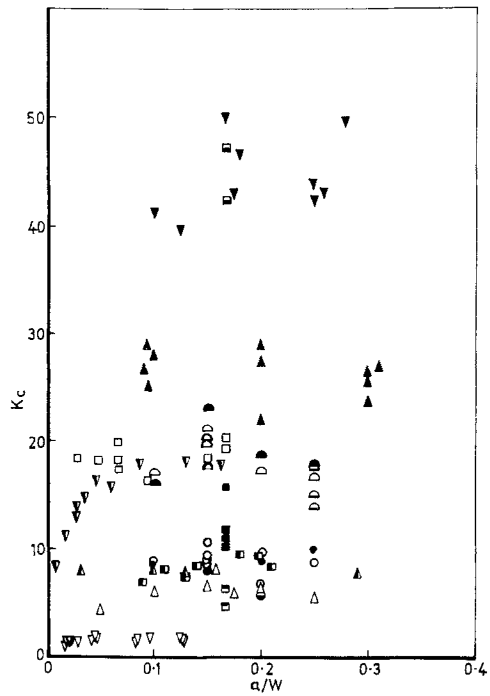

Figure 1 Survey of reported fracture toughness results.

The centre-notched (CN) specimens shown in Fig. 2 were used in both fracture toughness testing and fatigue crack propagation studies. For this geometry, the stress intensity factor, K, is given in [1] as

$$K = \sigma_G \sqrt{W}\left(\frac{a}{W}\right)^{\frac{1}{2}} \qquad (3)$$

$$\times \left[1.77 + 0.454\left(\frac{a}{W}\right) - 1.02\left(\frac{a}{W}\right)^2 + 5.4\left(\frac{a}{W}\right)\right]^3$$

where σ_G is the gross stress applied to the ends of the specimen. To calculate K_c, the peak value of σ_G reached during a test, σ_{cG}, was used in the above equation, with the half-length of the sawn crack, a_0.

The testing machines used for tensile and fracture toughness testing were either an Instron 1195, or a modified type "E" Tensometer, or a Denison T42(500 kN), according to availability, at cross-head speeds of about 1 mm min^{-1}. For 900 mm wide specimens, a 1000 kN machine was designed

TABLE II Description of materials

Abbreviation	Trade name	Description
CSM	Fibreglass Supremat	Chopped strand mat, E-glass, 450 g m^{-2}
WRF	Turner Bros. ECK25	Woven roving fabric, E-glass, 830 g m^{-2}, 197 ends/m warp, 158 ends/m weft
PR	B.P. Cellobond A2785CV	Polyester resin, isophthalic type containing: isophthalic acid, maleic anhydride, 1:2 propylene glycol; dissolved in styrene with added aerosil thixotrope and used with: catalyst: methyl ethyl ketone peroxide SD2; accelerator: 0.5% cobalt in styrene, NL48/ST

and build [24] (Fig. 3) which was also capable of applying pulsating load. For fatigue crack propagation tests on small specimens the 35 kN machines described by Owen [25] were used.

3. Fracture toughness results

Fracture toughness tests were carried out on dry and wet CN specimens of both materials, having $W = 50$, 100 and 150 mm, and with $a/W = 0.167$. Dry specimens were cut from 3-, 6- and 9-ply material. K_c was found to depend on the glass content and where there was sufficient variation, it was possible [24] to apply a linear relation between K_c and glass content and hence establish K_c for a standard glass content (35 wt% for CSM/PR, 65 wt% for WRF/PR). Where this was impossible, mean values of results were used. From Tables IV and V, the increase in K_c with W is much greater in WRF/PR than CSM/PR, but the reduction in K_c due to water absorption is only between 5 and 14% in both materials. There is only a negligible change in K_c with specimen thickness, which indicates that plane strain conditions are unlikely to be achieved, even in many plied laminates. The highly strained material at the crack tip will be trying to contract along the crack front. The less strained material adjacent to the crack front pre-

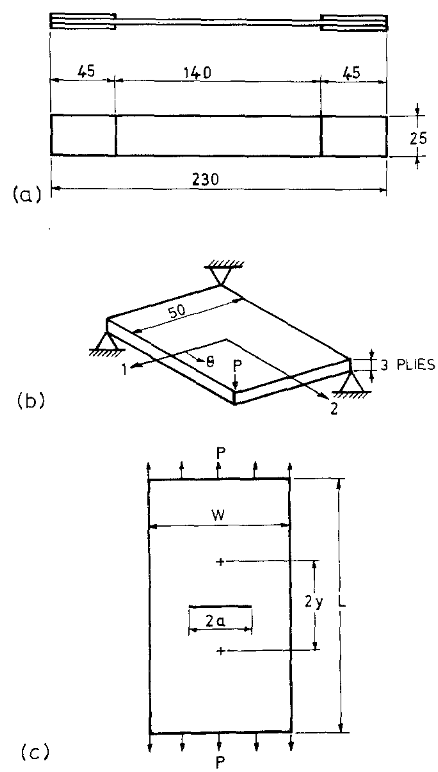

Figure 2 Specimens (dimensions in mm): (a) tensile; (b) plate twist; (c) centre notched (CN), $L/W = 2$, and $2y$ is the gauge length for the compliance gauge.

TABLE III Summary of ultimate tensile stress and compliances

Property		CSM/PR at glass content 35%	% change due to water absorption	WRF/PR at glass content 65%	% change due to water absorption
UTS	(MPa)	124.8	− 2.5	385.2	− 17.5
S_{11}	(GPa^{-1})	0.1004	+ 10.4	0.040 37	+ 2.1
S_{22}	(GPa^{-1})	0.1004	+ 10.4	0.040 37	+ 2.1
S_{12}	(GPa^{-1})	− 0.0399	− 6.9	− 0.008 23	+ 169.2
S_{66}	(GPa^{-1})	0.2805	+ 2.5	0.224 0	+ 16.3

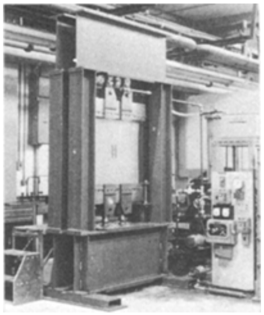

Figure 3 1000 kN capacity loading frame.

vents this and in a homogeneous yielding material plane strain conditions may be established. In GRP, the interfacial and interply strength is probably too low to support tensile forces along the crack front.

If K_c is a constant material property, from Equation 3 as $a_0/W \rightarrow 0$, $\sigma_{cG} \rightarrow \infty$. Clearly the failure stress of the material is an upper bound to σ_{cG}. Similarly, when $a_0/W = 0.5$, Equation 3 predicts a finite value for σ_{cG} when there is no material holding the specimen together. K_c cannot, therefore, be constant over the whole range of crack length. To see if a region existed between $a_0/W = 0$ and 0.5, where K_c was constant, 100 mm wide CN specimens of both materials were tested containing various length cracks. K_c, together with gross failure stress σ_{cG}, and nett failure stress σ_{cN}, are shown in Figs. 4 and 6. Use of the dimensionless forms $K_c/(\sigma_{UTS}\sqrt{W})$, σ_{cG}/σ_{UTS}, and σ_{cN}/σ_{UTS}, (where σ_{UTS} is that of the material around the crack, determined from the glass content of the material in this region), can be seen to reduce the scatter associated with glass content variation in the CSM/PR results (Figs. 4 and 5). In WRF/PR the glass content variation was smaller, so this procedure has little effect (Figs. 6 and 7).

In Figs. 4 to 7 it can be seen that K_c varies continuously with crack length. This behaviour was repeated in 915 mm wide specimens of CSM/PR (Fig. 8), but there appears to be a region where K_c may be reasonably constant with a/W. In Figs. 6 and 7, it can be seen that the nett section stress is constant in WRF/PR specimens, but not equal to the material ultimate tensile stress. Tests on a 100 mm wide specimen with no crack showed that this was caused by a stress concentration at the grips which proved more severe than the very short cracks. Failure of all WRF/PR specimens appeared to be by general simultaneous failure of the rovings, which tend to block crack propagation until their failure load is reached.

The failure of the 915 mm wide specimens of CSM/PR, occurred at very low stresses compared with the 100 mm specimens. The failure of all sizes of WRF/PR specimens occurred at about the same stress for a given crack length (Table VI). The load–displacement recording taken during the tests on the longest specimens was linear up to sudden failure. The failure of smaller specimens was less sharply defined.

TABLE IV Summary of mean K_c values and K_c values at 35% glass content, CSM/PR

Nominal width (mm)	Number of layers	Number of specimens	Mean K_c (MPa m$^{1/2}$)	35% glass content (MPa m$^{1/2}$)
CN 50 Dry	3	4	10.35	9.97
100	3	4	10.90	10.57
150	3	3	11.52	11.53
CN 50 Wet	3	5	8.63	8.67
100	3	5	9.92	10.04
150	3	5	10.14	10.60
CN 50 Dry	6	5	10.24	9.79
100	6	5	10.89	10.77
150	6	6	11.62	11.40
CN 50 Dry	9	5	10.26	10.26
100	9	5	10.96	10.67
150	9	6	12.08	11.23
CN 50 Dry	3, 6, 9	14	10.27	9.89
100	3, 6, 9	14	10.92	10.63
150	3, 6, 9	15	11.78	11.41

TABLE V Summary of mean K_c values and K_c values at 65% glass content, WRF/PR

Nominal width (mm)	Number of layers	Number of specimens	Mean K_c (MPa m$^{1/2}$)	65% glass content K_c (MPa m$^{1/2}$)
CN 50 Dry	3	4	35.89	35.84
100	3	4	46.13	43.83
150	3	4	55.31	50.63
CN 50 Wet	3	4	31.83	–
100	3	4	38.36	–
150	3	4	43.52	–
CN 50 Dry	6	3	28.42	–
100	6	2	39.87	–
50	9	3	31.40	–
CN 100 Dry	9	3	45.66	–
50	3, 6, 9	10	32.3	–
100	3, 6, 9	9	44.58	42.59

4. Fatigue crack propagation studies

Fatigue crack propagation tests were carried out on 100 mm wide CN specimens of both materials at a constant stress intensity factor range. Crack length was estimated from changes in specimen compliance, since damage obscured the position of the crack tip. Holdsworth and co-workers [11, 13] measured the compliance of several specimens containing sawn cracks of different lengths, but found that small compliance changes due to crack length were masked by variations in glass content. To obtain consistent results in the work described here, compliance in the dimensionless form (Ct/S_{11}) was related to crack length through the solution of a finite element model [24] similar to that described by Walters [27]. C is the specimen compliance measured between gauge points $2y$ apart (Fig. 2c), t the thickness, and S_{11} the normal

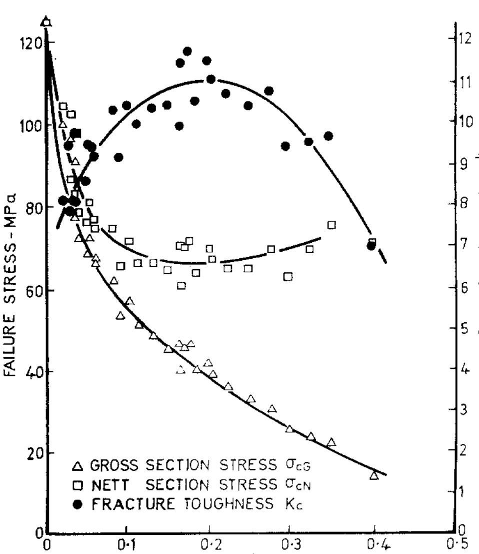

Figure 4 Change of fracture stress and fracture toughness with notch width, 100 mm wide CN specimens, CSM/PR material.

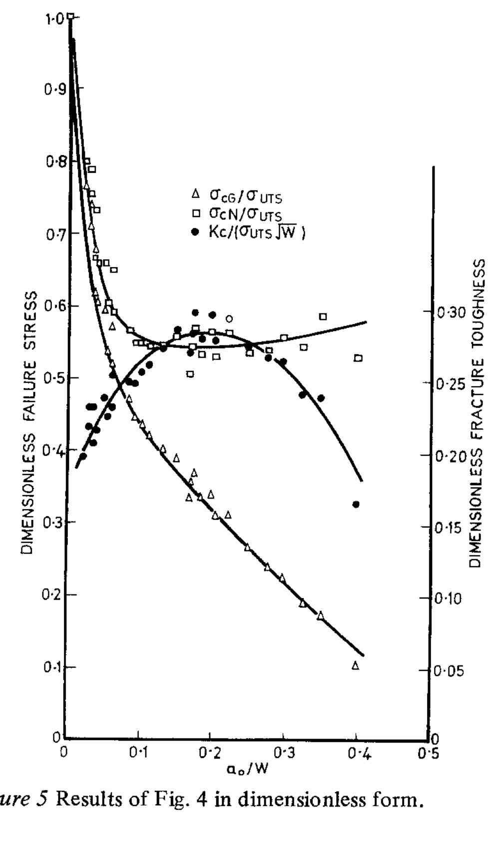

Figure 5 Results of Fig. 4 in dimensionless form.

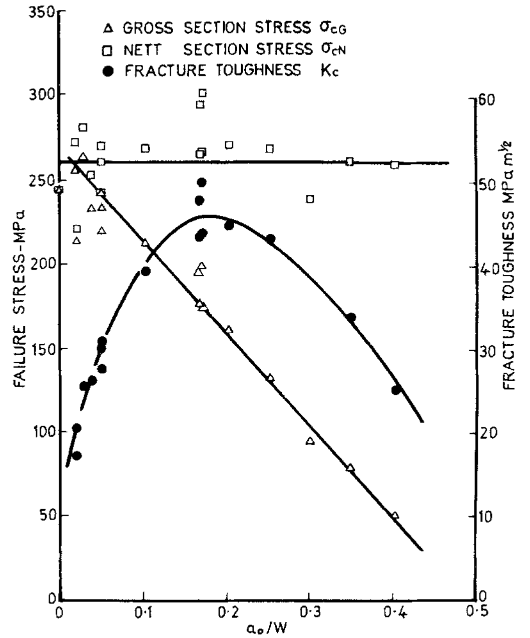

Figure 6 Change of fracture stress and fracture toughness with notch width, 100 mm wide specimens, WRF/PR material.

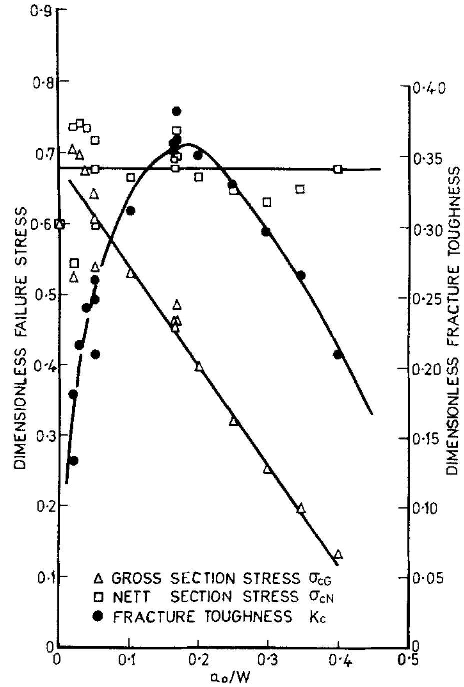

Figure 7 Results of Fig. 6 in dimensionless form.

material compliance ($= S_{22}$ in both materials, see Table III), of the material around the crack estimated from its glass content. In this form, the compliance was shown to be independent of glass content for isotropic and transversely orthotropic materials provided $2y$ is small. Computed specimen compliances agreed well with experimental compliances when expressed as Ct/S_{11}.

Initially, a load–displacement curve for the test specimen (maximum load 3 kN), was recorded on an $X-Y$ plotter and assigned a value of (Ct/S_{11}) corresponding to the measured crack length, from the specimen compliance–crack length relation. The specimen was then cycled at a load to give the desired value of stress intensity factor range (ΔK) for a few hundred cycles. The compliance was measured again and the new crack length found from the calibration. The load was reduced to keep ΔK constant and the cycling continued. This process was repeated until either the specimen broke, or a large number of cycles had been completed. The initial rate of crack growth was very high compared with the remainder of the test until just before failure.

Graphs of crack growth against cycles at various ΔK values for wet and dry CSM/PR and WRF/PR are shown in Figs. 9 to 11 and 13. Rates of growth are given in Tables VII, VIII and IX. The variation in glass content of the dry CSM/PR specimens caused crack growth to occur at a lower rate in specimens tested at higher ΔK than in specimens tested at an apparently lower ΔK. Expressing ΔK as $\Delta K/(\sigma_{\text{UTS}}\sqrt{W})$, where σ_{UTS} is found from the glass content, can be seen from Table VII to remove this anomaly.

In Fig. 9 it is difficult to distinguish regions

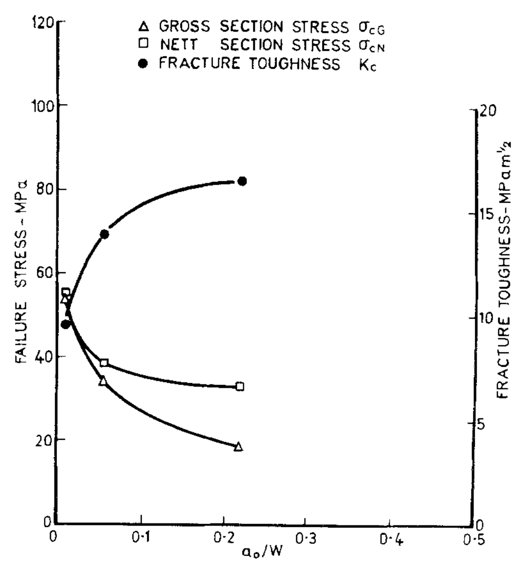

Figure 8 Change of failure stress and fracture toughness with notch width, 914 mm wide CN specimens, CSM/PR material.

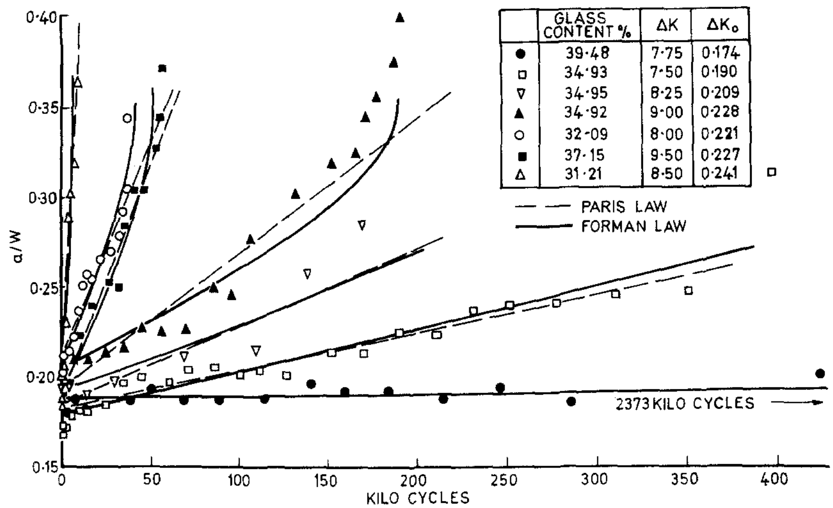

Figure 9 Fatigue crack growth in 100 mm wide CN specimens, dry CSM/PR material.

where $\mathrm{d}a/\mathrm{d}N$ is constant. The Paris fatigue crack propagation law, equation 2, predicts a finite growth rate at $\Delta K = K_c$. In Forman's law [26],

$$\frac{\mathrm{d}a}{\mathrm{d}N} = \frac{A\Delta K^m}{(K_c - \Delta K)} \quad (4)$$

$\mathrm{d}a/\mathrm{d}N \to \infty$ as $\Delta K \to K_c$ but K_c is assumed constant with a. In the previous section it was shown that K_c varies with a/W so that it is possible for K_c to approach the value of ΔK at which the specimen is being tested. A third-order polynomial was fitted to the $K_c/(\sigma_{\mathrm{UTS}}\sqrt{W})$ against a_0/W curve in Fig. 5 to express Equation 4 in the form

$$\frac{\mathrm{d}a_\mathrm{D}}{\mathrm{d}N} = \frac{A\Delta K_\mathrm{D}^m}{[B_0 - \Delta K_\mathrm{D}] + B_1 a_\mathrm{D} + B_2 a_\mathrm{D}^2} \quad (5)$$

where the B_0, B_1 and B_2 are constants, $a_\mathrm{D} = a_0/W$, $\Delta K_\mathrm{D} = \Delta K/(\sigma_{\mathrm{UTS}}\sqrt{W})$, which in a constant ΔK cycling test can be integrated to give [24]:

$$N - N_\mathrm{i} = k\left[(B_0 - \Delta K_\mathrm{D})(a_\mathrm{D} - a_\mathrm{Di}) + \frac{B_1}{2}(a_\mathrm{D}^2 - a_\mathrm{Di}^2) + \frac{B_2}{3}(a_\mathrm{D}^3 - a_\mathrm{Di}^3)\right] \quad (6)$$

where a_Di, N_i are initial values and

$$k = 1/A\Delta K^m. \quad (7)$$

The least squares method was used to determine a value of $1/k$ that gives a best fit for Equation 6 to the curves in Fig. 9. The solid lines in Fig. 9 are Equation 6 and the dotted lines assume $\mathrm{d}a/\mathrm{d}N$ is constant. The Paris law is equivalent to Forman's law at low rates of growth where ΔK is much less than K_c. For wet CSM/PR and WRF/PR (Figs. 10 and 13), because crack growth took place at low ΔK values relative to K_c, there were clearly defined regions where $\mathrm{d}a/\mathrm{d}N$ was constant.

The fatigue crack-growth resistance of WRF/PR is superior to CSM/PR and its mode of failure quite different. Horizontal crack growth is blocked by vertical rovings. There appear to be several distinct regions of growth rate in Fig. 11. The apparent horizontal crack growth which increases according to compliance measurements, is really growth of vertical cracks at the tips of the initial central crack (Fig. 12). When these have grown to a certain length, growth ceases until the horizontal rovings bridging the crack give way. This effectively divides the specimen into two separate ligaments. Failure follows in the next few thousand cycles. The growth rates in all regions were roughly independent of ΔK (Table VII) but Fig. 11 shows that the duration of the central region of low growth rate decreased with increasing ΔK. Application of either of the crack-growth laws mentioned above seems inappropriate.

Specimens that had undergone the water-absorption treatment were kept in a water bath during testing. The rate of crack growth at equivalent ΔK values increased by at least three orders of magnitude in CSM/PR specimens due to water absorption (Tables VII to IX). The mechanism in the WRF/PR specimens by which horizontal crack propagation is blocked and vertical cracks formed, is destroyed by prolonged water immersion and horizontal growth took place. Therefore, it was

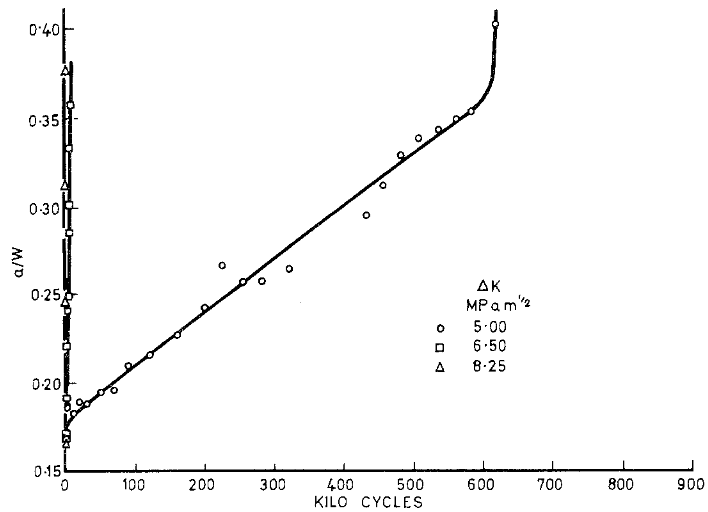

Figure 10 Fatigue crack growth in 100 mm wide CN specimens, wet CSM/PR material.

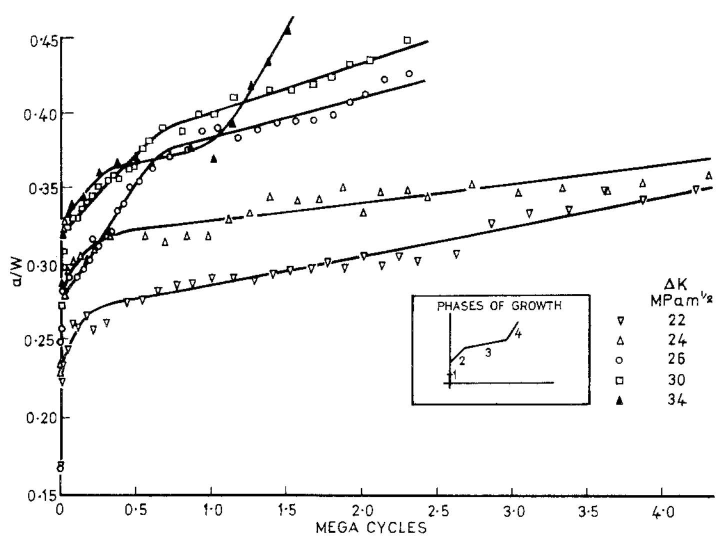

Figure 11 Fatigue crack growth in 100 mm wide CN specimens, dry WRF/PR material.

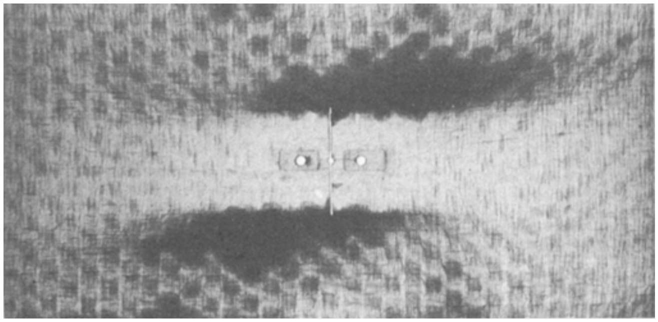

Figure 12 Crack tips in WRF/PR.

possible to apply the Paris law to wet WRF/PR (Fig. 13). $\mathrm{d}a/\mathrm{d}N$ and $1/k$ are plotted logarithmically against ΔK to obtain A and m in the crack growth laws, as in Fig. 14.

In summary, the crack growth in the various specimens could be represented by the following relationships.

For dry CSM/PR using the Paris law

$$\frac{\mathrm{d}a_\mathrm{D}}{\mathrm{d}N} = 3.37 \times 10^7 \Delta K_\mathrm{D}^{20.33} \qquad (8)$$

or

$$\frac{\mathrm{d}a}{\mathrm{d}N} = 1.19 \times 10^{-26} \Delta K^{20.33}$$

(at 35% glass content). (9)

For dry CSM/PR using the Forman law

$$\frac{\mathrm{d}a_\mathrm{D}}{\mathrm{d}N} = \frac{2.31 \times 10^3 \Delta K_\mathrm{D}^{15.97}}{K_\mathrm{Dc} - \Delta K_\mathrm{D}} \qquad (10)$$

or

$$\frac{\mathrm{d}a}{\mathrm{d}N} = \frac{2.94 \times 10^{-26} \Delta K^{15.97}}{K_\mathrm{c} - \Delta K}$$

(at 35% glass content) (11)

where K_c, K_Dc vary as shown in Figs. 7 and 8, respectively.

For wet CSM/PR using the Paris law

$$\frac{\mathrm{d}a_\mathrm{D}}{\mathrm{d}N} = 1.32 \times 10^5 \Delta K_\mathrm{D}^{12.86} \qquad (12)$$

or

$$\frac{\mathrm{d}a}{\mathrm{d}N} = 3.92 \times 10^{-17} \Delta K^{12.86}$$

(at 35% glass content). (13)

For wet WRF/PR using the Paris law

$$\frac{\mathrm{d}a_\mathrm{D}}{\mathrm{d}N} = 0.007\,94 \Delta K_\mathrm{D}^{5.6} \qquad (14)$$

or

TABLE VI Fracture toughness tests on 915 mm wide CN specimens, CSM/PR and WRF/PR

Half-crack length/ width ratio a/W	Gross stress at failure (MPa)	Nett stress at failure (MPa)	K_c (MPa m$^{1/2}$)
0.2187 CSM/PR	18.67	33.18	16.49
0.055 19	34.36	38.60	13.88
0.010 93	54.11	55.32	9.60
0.054 59 WRF/PR	232.91	261.46	93.68
0.219 90	183.25	327.12	161.98

TABLE VII Fatigue crack propagation tests, CSM/PR

ΔK (MPa m$^{1/2}$)	Glass content by weight (%)	ΔK_D	$\mathrm{d}a_\mathrm{D}/\mathrm{d}N$	Cycles to failure N_c
Dry 7.75	39.48	0.174	0.719×10^{-8}	2 373 000 S*
7.50	34.93	0.190	0.206×10^{-6}	397 640
8.25	34.95	0.209	0.421×10^{-6}	205 630
9.00	34.92	0.228	0.740×10^{-6}	190 530
8.00	32.09	0.221	0.234×10^{-5}	37 790
9.50	37.15	0.227	0.257×10^{-5}	56 300
8.50	31.21	0.241	0.195×10^{-4}	8 500
Wet 5.00	35.22	0.126	0.301×10^{-6}	614 050
6.50	33.89	0.170	0.249×10^{-4}	6 770
8.25	35.44	0.207	0.160×10^{-3}	1 890

* S indicates test stopped without failure occurring.

TABLE VIII Fatigue crack propagation tests, WRF/PR, dry

ΔK (MPa m$^{1/2}$)	Glass content by weight (%)	ΔK_D	$\mathrm{d}a_\mathrm{D}/\mathrm{d}N$ phase 2	$\mathrm{d}a_\mathrm{D}/\mathrm{d}N$ phase 3	Cycles to failure N_c
22	67.68	0.168	0.215×10^{-6}	0.195×10^{-8}	4 904 000 S*
24	67.66	0.184	0.148×10^{-6}	0.126×10^{-8}	4 268 179 S
26	64.71	0.215	0.155×10^{-6}	0.274×10^{-8}	2 287 000 S
30	66.95	0.234	0.101×10^{-6}	0.278×10^{-8}	2 503 260
34	65.52	0.275	0.112×10^{-6}	0.221×10^{-8}	1 493 400
		Mean value	0.146×10^{-6}	0.219×10^{-8}	

* S indicates test stopped without failure occurring.

TABLE IX Fatigue crack propagation tests, WRF/PR, wet

ΔK ($MPa\,m^{1/2}$)	Glass content by weight (%)	ΔK_D	da_D/dN	Cycles to failure N_c
14	65.46	0.114	0.402×10^{-7}	1 970 000 S*
18	65.96	0.144	0.166×10^{-6}	494 500
22	66.88	0.172	0.410×10^{-6}	271 680

* S indicates test stopped without failure occurring.

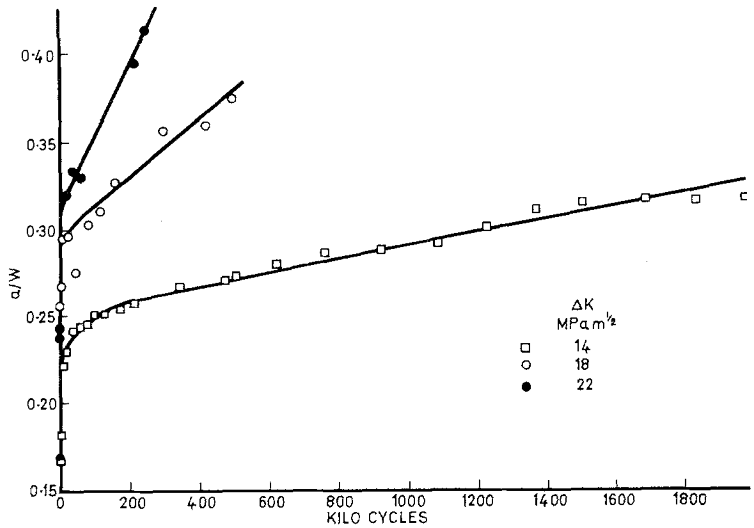

Figure 13 Fatigue crack growth in 100 mm wide CN specimens, wet WRF/PR material.

$$\frac{da}{dN} = 1.66 \times 10^{-15} \Delta K^{5.6}$$

(at 65% glass content). (15)

5. Conclusions

Clearly WRF/PR is the tougher of the two materials tested. The rovings prevent crack propagation, which causes the large increase in K_c with width. This size effect is much less in CSM/PR specimens. For the stress intensity approach to be applicable to GRP specimens they should be (i) of notch-sensitive material, and (ii) large enough for rapid crack propagation to be the dominant failure mode. Such failures have been observed in large GRP structures. Results from thin specimens can be applied to thicker material, (provided transverse buckling is restrained in the thin specimens). The effect of water absorption on fracture toughness is small and comparable with the reduction in strength. The survey shows that most GRP are selected for testing at random. Further work should examine the effect on fracture toughness of varying fibre, strand or roving diameter of the reinforcing material, keeping glass content constant. The J

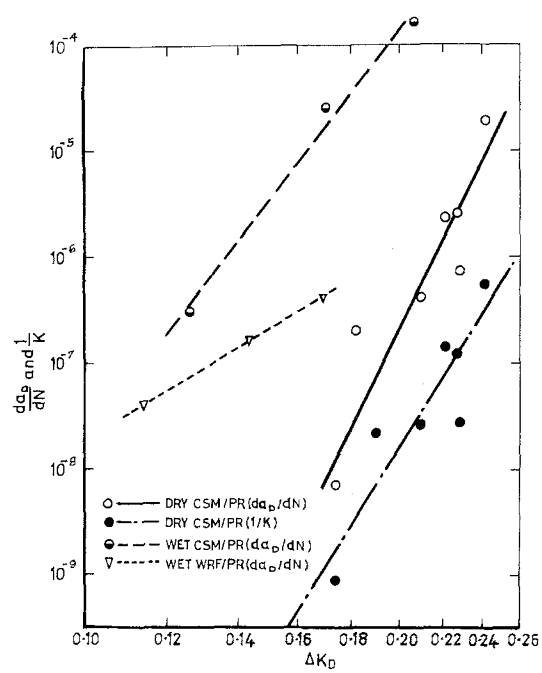

Figure 14 da_D/dN or $1/k$ against ΔK_D for the determination of constants in the crack-growth laws.

integral approach has been shown [28] to give J_c values that are independent of crack length but increase with specimen thickness. The latter may be due to transverse buckling which is known to affect K_c values. J_c may be closer to being a material constant than K_c, but it is difficult to see how, practically, it can be used to describe fatigue crack propagation.

The use of dimensionless forms of ΔK has been shown to eliminate scatter in fracture toughness results and explain apparently anomalous rates of growth observed in CSM/PR specimens. The use of Forman's law accounts for changing rates of growth at ΔK close to K_c. The Paris fatigue crack-growth law adequately describes low rates of growth but higher rates of growth are better described by Forman's law, allowing for variation in K_c with crack length. Neither law is applicable to WRF/PR unless it has been in water for a long period of time. The most important finding is the severe reduction in crack-growth resistance in both materials caused by water absorption.

Acknowledgement

This work has been carried out with the financial support of the Procurement Executive, Ministry of Defence.

References

1. P. C. PARIS and G. C. SIH, ASTM, STP 381, Philadelphia (1965) p. 30.
2. W. F. BROWN and E. SRAWLEY, ASTM, STP 410 (1966).
3. E. M. WU and R. C. REUTER, University of Illinois, Department of Theoretical and Applied Mechanics, Report No. AD-613 576 (1963).
4. R. J. SANDFORD and R. STONESIFIER, *J. Comp. Mat.* **5** (1971) 241.
5. P. W. R. BEAUMONT and D. C. PHILLIPS, *J. Mater. Sci.* 7 (1972) 682.
6. *Idem, J. Comp. Mater.* **6** (1972) 32.
7. F. MCGARRY and J. F. MANDELL, "Fracture Toughness Studies of Fibre Reinforced Plastic Laminates", Faraday Special Discussions of the Chemical Society, 2 (1972).
8. R. HAMILTON and C. BERG, *Fibre Sci. Technol.* **6** (1973) 55.
9. M. J. OWEN and P. T. BISHOP, *J. Comp. Mater.* **7** (1973) 146.
10. M. J. OWEN and R. G. ROSE, *J. Phys. D. Appl Phys.* **6** (1973) 42.
11. A. HOLDSWORTH, S. MORRIS and M. J. OWEN, *ibid* 7 (1974) 2036.
12. J. F. MANDELL, F. J. MCGARRY, S. S. WANG and J. IM, *J. Comp. Mater.* 8 (1974) 106.
13. A. W. HOLDSWORTH, Ph.D. Thesis, University of Nottingham (1973).
14. S. GAGAR and L. J. BROUTMAN, *Int. J. Fracture* **10** (1974) 606.
15. J. T. BARNBY and B. SPENCER, *J. Mater. Sci.* **11** (1976) 78.
16. N. FRIED, J. KAMINETSBY and M. SILVERGLEIT, "The Effect of Deep Submergence Operational Conditions on Filament Wound Plastics", 21st Annual Conf. Soc. of Plastics Industries Reinforced Plastics Division (1966).
17. R. C. WYATT and K. H. G. ASHBEE, *Fibre Sci. Technol.* **2** (1969–70) 29.
18. J. B. ROMANS, A. G. SANDS and J. E. COWLING, *Ind. Eng. Chem. Product Res. Devel.* **11** (1972) 261.
19. P. C. PARIS, Boeing Co. Document No. D-17867, Addendum N (1957).
20. R. W. HERTZBERG, J. A. MANSON and H. NORDBERG, Ohio State University Report No. AD-700434 (1963).
21. G. C. SIH, P. D. HILTON and R. P. WEI, Report No. AD-709 214 (1970).
22. P. A. THORNTON, *J. Comp. Mater.* **6** (1972) 147.
23. M. J. OWEN and P. T. BISHOP, *J. Phys. D. Appl. Phys.* 7 (1974) 1214.
24. R. J. CANN, Ph.D. Thesis, University of Nottingham, (1977).
25. M. J. OWEN, *Trans. J. Plastics Inst.* **35** (1967) 353.
26. R. G. FORMAN, V. E. KEARNY and P. M. ENGLE, *J. Basic Eng.* 89 (1967) 459.
27. J. V. WALTERS, Ph.D. Thesis, University of Nottingham (1975).
28. G. SMITH, A. K. GREEN and W. H. BOWYER, Proceedings of the Institute of Physics Stress Analysis Group, Annual Conference, Sheffield (1976) "Fracture Mechanics in Engineering Practice" (Applied Science, London, 1977) p. 271.

Received 28 November and accepted 18 December 1978.